

On the ring nebulae around runaway Wolf-Rayet stars

D. M.-A. Meyer^{*1}, L. M. Oskinova^{1,2}, M. Pohl^{1,3} and M. Petrov⁴

¹ *Universität Potsdam, Institut für Physik und Astronomie, Karl-Liebknecht-Strasse 24/25, 14476 Potsdam, Germany*

² *Department of Astronomy, Kazan Federal University, Kremlevskaya Str 18, Kazan, Russia*

³ *DESY, Platanenallee 6, 15738 Zeuthen, Germany*

⁴ *Max Planck Computing and Data Facility (MPCDF), Giesenbachstrasse 2, D-85748 Garching, Germany*

Received; accepted

ABSTRACT

Wolf-Rayet stars are advanced evolutionary stages of massive stars. Despite their large mass-loss rates and high wind velocities, none of them display a bow shock, although a fraction of them are classified as runaway. Our 2.5-D numerical simulations of circumstellar matter around a $60 M_{\odot}$ runaway star show that the fast Wolf-Rayet stellar wind is released into a wind-blown cavity filled with various shocks and discontinuities generated throughout the precedent evolutionary phases. The resulting fast-wind slow-wind interaction leads to the formation of spherical shells of swept-up dusty material similar to those observed in near-infrared $24 \mu\text{m}$ with *Spitzer*, and which appear to be co-moving with the runaway massive stars, regardless of their proper motion and/or the properties of the local ambient medium. We interpret bright infrared rings around runaway Wolf-Rayet stars in the Galactic plane, like WR138a, as indication of their very high initial masses and a complex evolutionary history. Stellar-wind bow shocks become faint as stars run in diluted media, therefore, our results explain the absence of detected bow shocks around Galactic Wolf-Rayet stars such as the high-latitude, very fast-moving objects WR71, WR124 and WR148. Our results show that the absence of a bow shock is consistent with a runaway nature of some Wolf-Rayet stars. This questions the in-situ star formation scenario of high-latitude Wolf-Rayet stars in favor of dynamical ejection from birth sites in the Galactic plane.

Key words: MHD – radiative transfer – methods: numerical – stars: circumstellar matter.

1 INTRODUCTION

The evolution of massive stars is poorly understood. It is characterised by the release of forceful winds whose intensity increases as the stars evolve. Strong wind interact with the local interstellar medium (ISM), leading to the formation of circumstellar wind bubbles structured by several shocks and discontinuities (Weaver et al. 1977). These pc-scale shells reflect both wind and ISM properties. They constitute the imprint of the past stellar evolution of massive stars onto their ambient medium (Meyer et al. 2014). Particularly, high-mass stars are expected to evolve through the so-called Wolf-Rayet (WR) phase. Despite the growing consensus on Galactic WR stars as the last pre-supernova evolutionary phase of $\geq 20 M_{\odot}$ stars, the precise evolutionary channels leading to such stellar objects remain uncertain (Crowther 2007). This stage is characterised by very strong winds enriched in C, N or O that are blown from the stellar surface with velocities up to $3000\text{--}5000 \text{ km s}^{-1}$ and large mass-loss rates reaching $10^{-5} M_{\odot} \text{ yr}^{-1}$ (Hamann et al. 2006; Bestenlehner et al. 2014; Sander et al. 2012).

WR stars often live in binary systems or have a binary evolu-

tionary history. These evolved stars have most likely travelled away from their birth place in the Galactic plane, either after many-body gravitational interaction within stellar groups or under the influence of the kick given by the shock wave of a defunct binary companion which ended its life as a supernova explosion (Moffat & Seggewiss 1979; Dinçel et al. 2015). However, only a handful of runaway WR stars are known in the Galaxy. This could be because the measurement of the radial velocity is complicated for WR optical spectra dominated by broad emission lines. Therefore, often the position of a WR star in the high-latitude region of the Milky Way serves as the primary indication of its runaway nature. The three most-studied high-galactic latitude WR stars are the binary WR 148 (WN8+B3IV, Munoz et al. 2017), WR 124 together with its suspected relativistic companion (WN8h, Toalá et al. 2018, and references therein), and WR 71 (WN6, Moffat et al. 1998).

The traditional method to discover runaway stars involves observations of bow-shocks. Indeed, one could expect that fast-moving WR stars are prone to produce bow shock nebulae (Wilkin 1996) under the conjugated influence of both their fast, dense stellar winds and their rapid bulk motion. This picture has been supported by several numerical hydrodynamical investigations of WR wind-ISM interaction predicting either the formation of un-

* E-mail: dmameyer.astro@gmail.com

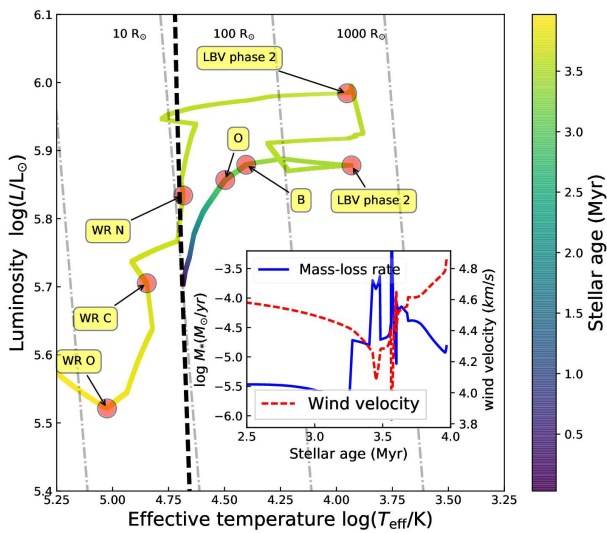


Figure 1. Evolutionary track of a star with an initial mass of $60 M_{\odot}$ (Groh et al. 2014). Inset: mass-loss rate and wind velocity for the post-main-sequence phases.

Table 1. Simulation models. Listed are the space velocity of the star, v_{\star} , and its ambient-medium number density, n_{ISM} .

Model	v_{\star} (km s $^{-1}$)	n_{ISM} (cm $^{-3}$)
Run-v30-n0.79	50	0.79
Run-v100-n0.79	100	0.79
Run-v200-n0.01	200	0.01

stable bow shocks (van Marle et al. 2005) or unstable ring-like shells (Brighenti & D’Ercole 1995a). However, no observational evidence of a bow shock around a WR star has been reported so far. On the other hand, WR stars are commonly surrounded by nebulae with a variety of morphologies, including ring-nebulae (Miller & Chu 1993; Marston 1997; Toalá et al. 2015) that have been observed in optical $H\alpha$ and [O III] lines as well as in the mid-infrared (Barniske et al. 2008). Recently, WR nebulae have been observed in the mm range (Fenech et al. 2018). Gräfenner et al. (2012) pointed out the prevalence of nebula around WR stars that only recently entered this evolutionary stage.

Interestingly, even fast moving WR stars (with velocities up to $v_{\star} \simeq 200 \text{ km s}^{-1}$ relative to the ISM) are located at the center of compact spherical shells (Gvaramadze et al. 2010). The question is therefore why fast-moving WR stars do not produce bow shock nebulae at all? How can their surroundings be shaped as a stable, circular shell? And why are those stars systematically centered onto those ring-like shells which appear to be co-moving with the star?

To answer these questions, we investigate the morphology of the circumstellar medium around evolving runaway WR stars by means of two-dimensional magneto-hydrodynamical and radiative transfer simulations. This study is organized as follows. We review the numerical models in Section 2, present the ring nebulae models in Section 3, discuss their significances in Section 4 and draw conclusions in Section 5.

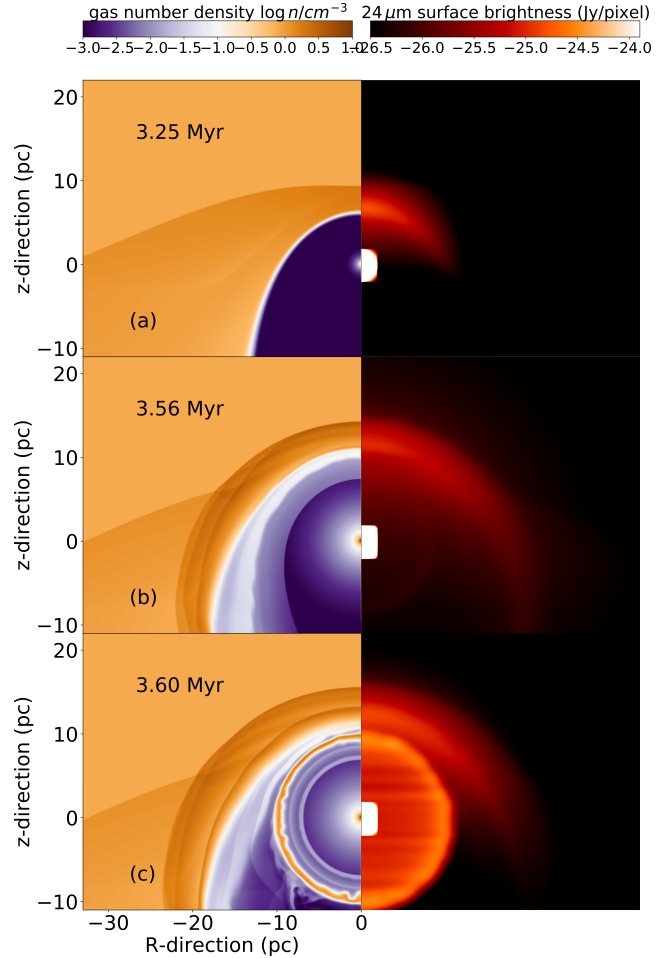


Figure 2. Density (left) and infrared 24- μm emission maps (right) of the circumstellar medium around a star with initial mass $60 M_{\odot}$ and evolving along the evolutionary track shown in Fig. 1. It plots the results for the model Run-v30-n0.79 in which the star moves with velocity 30 km s^{-1} in a medium of number density 0.79 cm^{-3} which corresponds to the warm phase of the Galactic plane. From top to bottom, selected snapshots are displayed, with the steady-state bow shock of the runaway star’s main-sequence phase (a); the “Napoleon’s hat” developing during the B-type phase of its stellar evolution and making room for the slow LBV materials to expand inside of it (b); the LBV material swept-up as a mid-infrared ring nebula by the fast WR wind (c). The spherical ring is brighter than the bow shock generated by the pre-WR winds.

2 NUMERICAL SIMULATIONS

We perform a series of 2.5D magneto-hydrodynamical (MHD) simulations with the PLUTO code (Mignone et al. 2012). The simulation have been carried out using a cylindrical coordinate system (R, z) mapped with a uniform grid $[z_{\text{min}}; z_{\text{max}}] \times [0; R_{\text{max}}]$ of resolution $\Delta = 0.08 \text{ pc cell}^{-1}$ minimum. A stellar wind is injected in the computational domain as a half sphere of radius 20 cells centered onto the origin, and a continuous inflow is set at the $z = z_{\text{max}}$ boundary so that the wind-ISM interaction is modelled in the frame of reference of the moving star (Meyer et al. 2016). We consider the ISM material to be at solar metallicity (Asplund et al. 2009). Energy loss/gain by optically-thin radiative cooling and heating are taken into account using a cooling law for a fully ionized medium (Meyer et al. 2014). Its equilibrium temperature is about 8000 K , i.e. we assume that the ambient medium is ionized

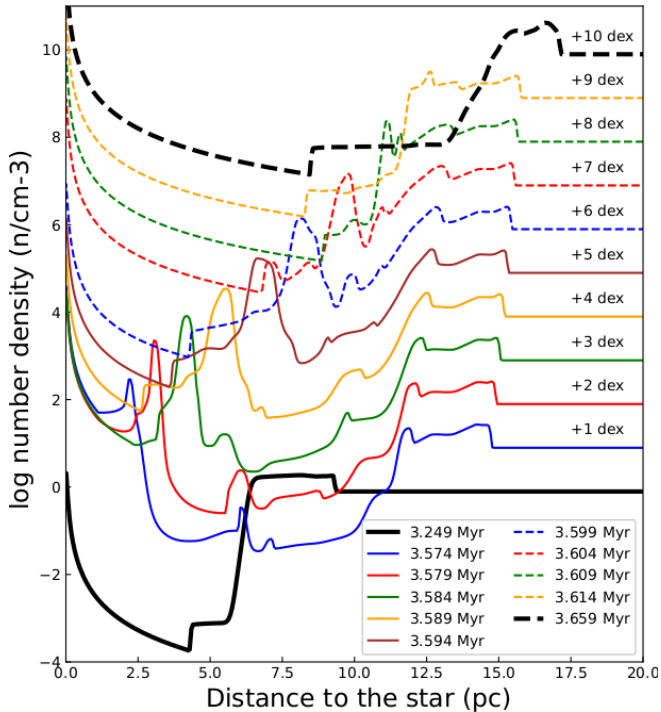


Figure 3. Number density profiles (in cm^{-3}) taken along the direction of motion of the runaway star, at selected times (in Myr) before, during and after the release of the WR WN shell. Each profile is offset by 1 dex.

by the strong stellar radiation field (Mackey et al. 2015). We assume the stars to move parallelly to the local ISM magnetic field of strength $7 \mu\text{G}$ (van Marle et al. 2014; Meyer et al. 2017).

We performed a series of 3 numerical simulations. Two ionized ISM are considered, with densities corresponding to either the Galactic plane ($n_{\text{ISM}} = 0.79 \text{ cm}^{-3}$) and to the high Galactic latitudes ($n_{\text{ISM}} = 0.01 \text{ cm}^{-3}$). Stars move therein with typical space velocity of $30\text{--}100 \text{ km s}^{-1}$ (Renzo et al. 2019) or 200 km s^{-1} , respectively. We use the stellar-evolution model for a non-rotating $60 M_{\odot}$ star of Groh et al. (2014). The track follows the stellar evolution from the zero-age-main-sequence through a B supergiant stage, a luminous-blue-variable (LBV) stage, characterized by a few eruptions, and finally the WR phase (Fig. 1). Our simulation parameters are summarised in Table 1.

We further post-process our MHD models with the code RADMC-3D (Dullemond 2012) that calculates the radiative transfer against dust opacity. The dust density field is constructed from the MHD models assuming a standard dust-to-gas mass ratio of $1/200$, and the dust temperatures are calculated by Monte-Carlo simulations. Following Green et al. (2019), the ionized stellar winds and gas hotter than 10^6 K is considered dust-free. Synthetic infrared images are then produced by ray-tracing stellar photons from the stellar atmosphere through the stellar surroundings. The star is assumed to be a spherical blackbody of effective temperature T_{eff} , bolometric luminosity L_{\star} , and radius R_{\star} interpolated from the stellar evolution track of Groh et al. (2014). We use opacities for a dust mixture based on silicates crystals (Laor & Draine 1993).

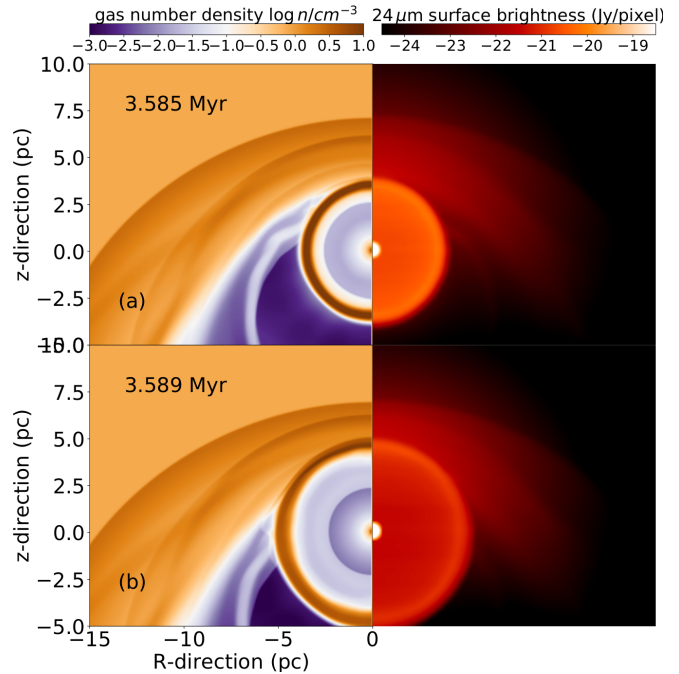


Figure 4. Same as Fig. 2 for the model Run-v100-n0.79. The $60 M_{\odot}$ star moves with velocity 100 km s^{-1} in a medium of number density 0.79 cm^{-3} , corresponding to the warm phase of the Galactic plane. From top to bottom, the images show that the fast wind-slow wind interaction generates a ring nebula around the fast moving WR star in the Galactic plane (a); and illustrates how the pre-WR evolution of the runaway star engenders series of arcs and filaments in the main-sequence bow shock (b). This compares well with the $\text{H}\alpha$ surroundings of WR 16 (left panel of Fig. 1 in Toalá & Guerrero 2013).

3 RESULTS

Fig. 2-7 illustrate the results in our numerical models. Fig. 2 displays the gas number density (in cm^{-3}) of our model Run-v30-n0.79 plotted in logarithmic scale (left-hand panels) and the corresponding *Spitzer* $24\text{-}\mu\text{m}$ infrared emission maps (right-hand panels). To be noted from the figure is that the wind-ISM interaction generates a steady-state MHD bow-shock system composed of an inner termination shock and an outer forward shock engulfing two regions of hot, low-density stellar wind and cold, dense shocked ISM (Meyer et al. 2017). In Fig. 2b one sees that the wind material of the B-type phase passes through the main-sequence bow shock and produces the appearance of a Napoleon’s Hat surrounding a cavity of low-density stellar wind.

Density profiles along the symmetry axis of model Run-v30-n0.79 taken at selected times are shown in Fig. 3. The solid thin blue line illustrates the stellar surroundings at the WR time, with the expanding wind (0-2 pc), the WR shell (2-2.5 pc), the successive cold/hot/cold LBV phases engendering two shells (5.5-7.5 pc), the shock front of B spectral type that has reached and pushed outwards the former main-sequence stellar wind bubble (10-12.5 pc). From time 3.579 Myr the WR shell keeps on expanding (Fig. 2b,c), reach (3.609 Myr) and merges (3.614 Myr) with the shocked layers of O-type and B-type wind material. At later times (dotted black line), the WR material has merged with the main-sequence bow shock.

Fig. 4 is as Fig. 2 but for our model Run-v100-n0.79, i.e. a star with velocity $v_{\star} = 100 \text{ km s}^{-1}$. The shaping of the circumstellar medium happens in a similar way, with a WR ring nebula devel-

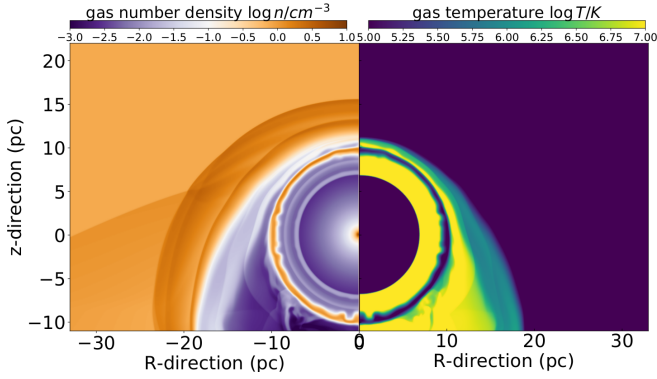


Figure 5. Density field (left) and temperature map of the shocked pre-WR wind and ISM materials (right) in our model Run-v30-n0.79 at time 3.6 Myr. The right-hand image shows the temperature map of the shock materials (inner shocked pre-WR stellar winds and outer shocked main-sequence and ISM gas). For clarity, the hot WR freely-expanding wind and the unperturbed ISM have been subtracted from the image. The swept-up LBV material is colder than its direct surroundings. Only the ring nebula together with the stellar wind bow shock have $T \leq 10^6$ K and can contain unsublimated dust particles. The other regions are therefore excluded from the radiative transfer calculations.

oping inside the cavity of slow LBV gas (Fig. 4a). As an effect of the faster stellar motion, no Napoleon’s hat forms and the ring interacts sooner with the bow shock since its stand-off distance is smaller (Wilkin 1996). Such a ring does not behave like regular bow-shock-producing material, and a bright arc-like nebula does not form, as is evident in the infrared emission maps in Fig. 2–6, as a consequence of the dust spatial distribution. Fig. 5 illustrates the location of the dust in the nebulae. It plots the gas density field (left, in g cm^{-3}) and the corresponding shocked material distribution (right, in K). The portion of the ring that collides with the termination shock upstream of the stellar motion becomes denser, although its overall circular shape is conserved.

Fig. 6 is the same as Fig. 2 but for our model Run-v200-n0.01. The star moves at very high speed in a diluted medium taken to be 0.01 cm^{-3} , which is typical of the low-density found in and above the Galactic plane. Consequently, the stand-off distance of the pre-WR bow shock is huge, about 20 pc, and so is the cavity of low-density stellar wind embedded inside of it. The shell of the fast WR wind expands into it and assumes the shape of a ring-like nebula. Due to the very extended shape of the bow shock, the ring has lots of space and time to expand, and consequently the Rayleigh-Taylor instability develops. The curvature of the unstable WR ring is modified once it interacts with the contact discontinuity produced during the previous evolutionary phase; it adopts a somewhat oblate morphology with higher density upstream of the stellar motion. This mechanism naturally holds for high latitudes above the Galactic plane where the ISM density is dilute, which makes the bow shock fainter and emphasizes the process of ring formation.

Note that the 2.5D nature of the MHD simulations implies a rotation of the solution around the Oz axis of the computational domain when interfacing the MHD bow shock model with the radiative transfer code. Consequently, the projection of the Rayleigh-Taylor-unstable ring nebulae induces a series of stripe-like features in the infrared emission map (right-hand part of Figs. 6b,c), see also Meyer et al. (2016). The detailed structure of the apex of MHD bow shocks might also be affected by the axis of symmetry as it can induce a concave-inward form that differs from the classical shape of stellar-wind bow shocks, see Figs. 6b and Fig. 1 of Meyer et al.

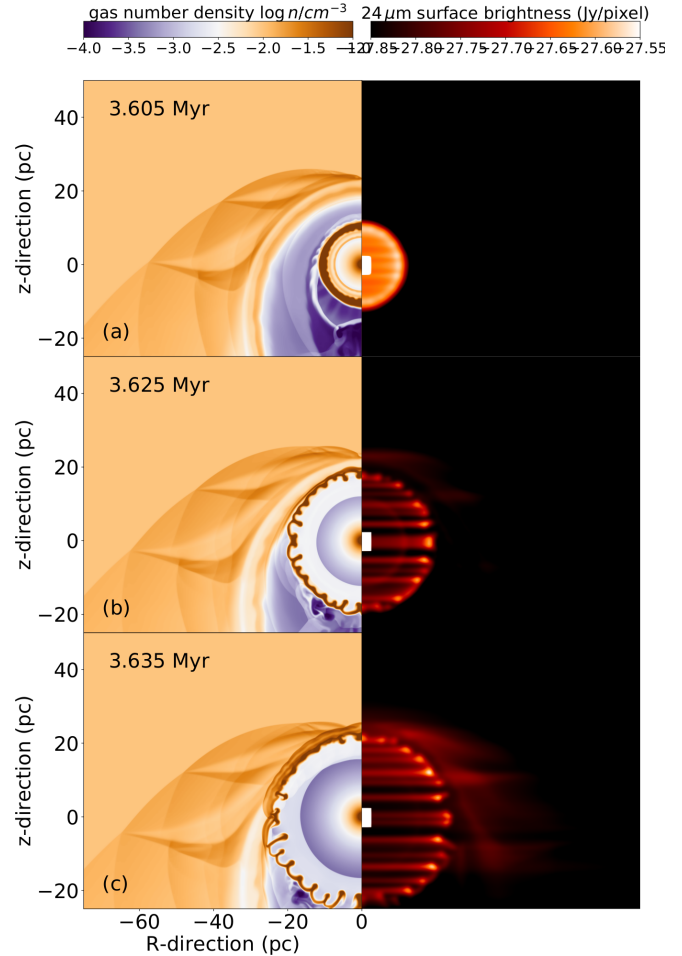


Figure 6. Same as Fig. 2 but for our model Run-v200-n0.01. The star moves with velocity 200 km s^{-1} in a medium of number density 0.01 cm^{-3} , corresponding to the dilute phase of the Galactic plane and/or to the higher latitude region above the Galactic disc. As the medium is diluted, the bow shock generated by the runaway star is huge and its infrared signature is faint, respectively (b). The region filled by slow LBV material is large, which permits to the ring swept-up by the fast WR wind to expand spherically despite of the driving star’s huge bulk velocity. This simulation model has qualitative properties in accordance with the WR 124 and its surrounding nebular structure M1-67 (van der Sluys & Lamers 2003).

(2017). Similarly, artefacts can develop in the trail of bow shock nebulae when gas accumulates and pills-off along the symmetry axis, see Fig. 5 of (Meyer et al. 2020). However, the latter does not affect our results. Circumventing those 2.5D-induced artefacts would require computationally-intensive full 3D MHD models.

In Fig. 7 we show the velocity profile along the direction of motion of the star at an early time of ring expansion in our model Run-v30-n0.79. The successive wind phases carve the main-sequence bow shock, making room for the *fast* WR wind to expand into a *slower* medium harboring multiple shocks and discontinuities of cold/hot LBV and earlier-type wind, hence producing a ring nebula. As the speed of the slow gas in the cavity is still larger than the stellar bulk motion, the ring seems to be co-moving with the runaway star.

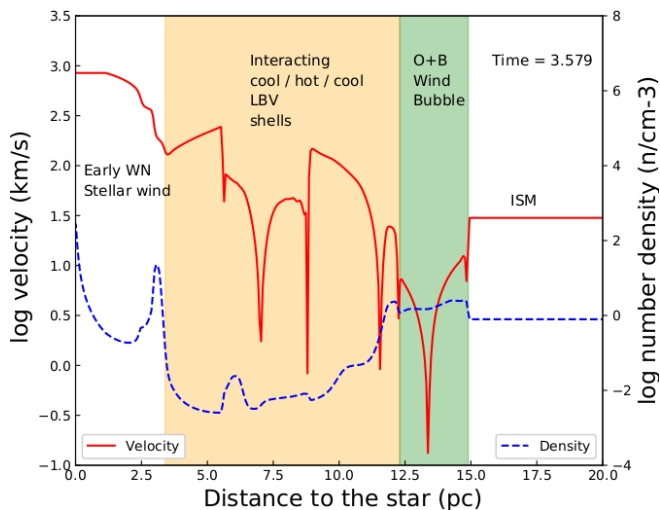


Figure 7. Profiles of gas velocity (in km s^{-1}) and number density taken along the direction of motion of the runaway star at time 3.579 Myr in our model Run-v30-n0.79, that involves a star moving at 30 km s^{-1} (see also Fig. 3). The orange and green regions highlight the regions mostly made of LBV or O/B material. Note that additional mixing may happen.

4 DISCUSSION

In this paper, we presented numerical models for the circumstellar medium of very massive runaway stars. For a star with initial mass of $60 M_{\odot}$ stars that follows an evolutionary path successively characterised by phases with O and B spectral type, multiples cold/hot LBV eruptions, and several final WR phases (Groh et al. 2014), we investigate the formation of ring-like nebulae. Our simulations show that the stellar wind remains confined inside its main-sequence wind bubble. We calculate the radiative transfer against dust opacity in the stellar environment and demonstrate that the ring-formation mechanism discussed above explains the systematic centering of circumstellar shells surrounding many evolved massive stars such WR stars, that are observed as mid-infrared circular circumstellar nebulae (Gvaramadze et al. 2010).

Previous models of $20\text{--}30 M_{\odot}$ runaway WR stars assumed a simpler evolution through a red-supergiant phase. They indicated that the early WR wind expands spherically before eventually interacting directly with the ISM, once the WR ring passed through the relatively compact red supergiant bow shock (Brighenti & D’Ercole 1995b; van Marle et al. 2005). The shells of WR wind get rapidly distorted once they interact with the ISM. For very massive stars, the rings develop in much larger cavities, and therefore the observation of a ring co-moving with very fast runaway WR stars is the consequence of a complex stellar evolution involving series of LBV eruptions. This constrains the star’s initial mass to $> 40 M_{\odot}$, i.e. to the mass range of stars which do not directly evolve to the WR stage via a single red supergiant phase.

Inside the wind-blown bubble, the post-main-sequence winds generate a pattern of various shocks and unstable discontinuities separating slow, dense, and cold gas from hot and fast material that collide with each other, creating a cavity of slow stellar wind inside of which the fast WR material is released. Star-centered rings such as the nebula surrounding WR71 are far denser and closer to the star than the bow shock, and consequently they appear brighter in dust-scattered starlight than the bow shock itself (Faherty et al. 2014; Flagey et al. 2014). LBV winds are often anisotropic. Older rings may therefore lose their early sphericity on account of propagation

in an anisotropic wind zone, which explains the variety of observed shells (Gvaramadze et al. 2010; Stock & Barlow 2010).

For slower stars moving in the Galactic plane, a Napoleon’s hat forms on account of multiple arced structures arising from the succession of different phases (Fig. 2). Another trace of complex pre-WR evolution are the series of arcs produced in the main-sequence bow shock when the various winds interact with the termination shock (Figs. 4 and 6). The aftermath of the succession of mass-loss events is visible at $H\alpha$ in the vicinity of WR 16’s shell, see left panel of Fig. 1 in Toalá & Guerrero (2013).

Our simulations compare well with high-latitude runaway WR stars. The properties of the early WN type star WR 124 with its nebular structure M1-67 and the star WR 148, both moving at velocities $v_{*} \approx 200 \text{ km s}^{-1}$, resemble our Run-v200-n0.001. WR 124 is not surrounded by a circular ring but a series of clumps, filaments and arcs, suggesting that the star just entered the WN phase and that no swept-up dust material has formed yet. Associating the arcs to LBV ejections, van der Sluys & Lamers (2003) derived the presence of a large-scale bow at 1.3 pc from the star. Such a small stand-off distance is in conflict with our model as we obtain $\approx 20 \text{ pc}$, however using an ISM density of $n_{\text{ISM}} \approx 0.01 \text{ cm}^{-3}$ while the authors assumed $n_{\text{ISM}} \approx 1.0 \text{ cm}^{-3}$ which we deem too large for a high-latitude star. WR 124’s bow shock is located at a larger distance and it is therefore much fainter compare to the nebular shell M1-67.

WR 148 has similar altitude and proper motion as WR124 but displays neither a bow shock nor a detected nebula. Our models suggest that the existing ring nebula is too young to be seen at such distance ($> 8 \text{ kpc}$) and that a large, faint bow shock should surround it. Our model Run-v200-n0.01 assumes the highest known stellar velocity of a WR star, but a very dilute medium. Any star located higher above the Galactic disk will naturally produce an even larger cavity of slow stellar wind and rings of swept-up hot material (Rate & Crowther 2020). This explains the systematic absence of observed bow shocks around high-latitude runaway WR stars. They are too large, diluted and faint to be detected, despite their huge proper motion and significant mass-loss rate (Toalá et al. 2015). Finally, our models explain the circumstellar structures around high high-latitude WR stars without assuming their in-situ formation.

Last, the duration of the LBV phase might affect the development of the ring nebula. The stellar evolution model of Groh et al. (2014) assume a rather long LBV phase of $2.35 \times 10^5 \text{ yr}$, while much shorter LBV phases exist. e.g. in the case of lower-mass ($20\text{--}25 M_{\odot}$) progenitors (Chita et al. 2008; Groh et al. 2013) or at lower-metallicity such as in the Large Magellanic Cloud (Bohannon 1997). Shorter LBV eruptions will supply the interior of the bow shock with less material, and, consequently, diminish the amount of material accumulated in the ring that will become thinner as it expands outwards. This might affect our results, as long as the star is at rest or moves slowly (Meyer et al. 2020), whereas if it moves fast and/or in a dense medium the stand-off distance of the bow shock is short and less LBV material is required to generate a ring nebulae that will last less time. The length of the WR phase does not matter in the ring production as it acts as a source of momentum that sweeps up the LBV material. All these elements are consistent with the conclusions of Gräfener et al. (2012) who found that ring nebulae are mostly observed around early-type WR stars.

The models presented in this paper are computed of one particular stellar-evolution model (Groh et al. 2014). The formation of ring nebulae around runaway WR stars should qualitatively remain

the same regardless of the details of its evolution history, as long as the star undergoes episodes of faster and slower winds and ejects a considerable amount of mass after its main-sequence phase (such as a LBV mass ejections).

5 CONCLUSION

Our simulations change the paradigm of the surroundings of WR stars and reveal a complex picture the formation of WR ring nebulae. In the Galactic plane, the same fast wind-slow wind interaction mechanism is responsible for the formation of observed near-infrared ring nebulae appearing to be co-moving with some runaway WR stars (Gvaramadze et al. 2010), as long as a sufficiently complex evolution via, e.g., a B spectral-type phase and LBV eruptions happen and enlarge the wind cavity. The presence of infrared rings, that are brighter than the bow shock, therefore reflect a very large ($> 40 M_{\odot}$) initial mass of these WR stars.

The absence of detected bow shocks and the presence of diffuse ring nebulae around high-Galactic-latitude WR stars does not imply the nonexistence of supersonic stellar motion though the ISM, because that would produce a distant and very faint bow shock. Our study motivates further high-resolution, multi-wavelength observational campaigns of the circumstellar medium of Galactic WR stars such as the 3-mm interferometric ALMA observations of Westerlund 1 (Fenech et al. 2018) or the observations of non-thermal radio emission of WR wind bubble G2.4+1.4 (Prajapati et al. 2019), in order to unveil their detailed structures and to constrain the late evolution of their driving star.

ACKNOWLEDGEMENTS

The authors acknowledge the North-German Supercomputing Alliance (HLRN) and the Max Planck Computing and Data Facility (MPCDF) for providing HPC resources. LMO acknowledges financial support by the Deutsches Zentrum für Luft und Raumfahrt (DLR) grant FKZ 50 OR 1809, and partial support by the Russian Government Program of Competitive Growth of Kazan Federal University.

REFERENCES

- Asplund M., Grevesse N., Sauval A. J., Scott P., 2009, *ARA&A*, 47, 481
 Barniske A., Oskinova L. M., Hamann W. R., 2008, *A&A*, 486, 971
 Bestenlehner J. M., Gräfener G., Vink J. S. e. a., 2014, *A&A*, 570, A38
 Bohannan B., 1997, in Nota A., Lamers H., eds, *Luminous Blue Variables: Massive Stars in Transition* Vol. 120 of *Astronomical Society of the Pacific Conference Series*, The Definition of Luminous Blue Variable. p. 3
 Brighenti F., D’Ercole A., 1995a, *MNRAS*, 277, 53
 Brighenti F., D’Ercole A., 1995b, *MNRAS*, 273, 443
 Chita S. M., Langer N., van Marle A. J., García-Segura G., Heger A., 2008, *A&A*, 488, L37
 Crowther P. A., 2007, *ARA&A*, 45, 177
 Dinçel B., Neuhäuser R., Yerli S. K., Ankaý A., Tetzlaff N., Torres G., Mugrauer M., 2015, *MNRAS*, 448, 3196
 Dullemond C. P., 2012, *RADMC-3D: A multi-purpose radiative transfer tool*, *Astrophysics Source Code Library*
 Faherty J. K., Shara M. M., Zurek D., Kanarek G., Moffat A. F. J., 2014, *AJ*, 147, 115
 Fenech D. M., Clark J. S., Prinja R. K., Dougherty S., Najarro F., Negueruela I., Richards A., Ritchie B. W., Andrews H., 2018, *A&A*, 617, A137
 Flagey N., Noriega-Crespo A., Petric A., Geballe T. R., 2014, *AJ*, 148, 34
 Gräfener G., Vink J. S., Harries T. J., Langer N., 2012, *A&A*, 547, A83
 Green S., Mackey J., Haworth T. J., Gvaramadze V. V., Duffy P., 2019, *A&A*, 625, A4
 Groh J. H., Meynet G., Ekström S., 2013, *A&A*, 550, L7
 Groh J. H., Meynet G., Ekström S., Georgy C., 2014, *A&A*, 564, A30
 Gvaramadze V. V., Kniazev A. Y., Fabrika S., 2010, *MNRAS*, 405, 1047
 Hamann W. R., Gräfener G., Liermann A., 2006, *A&A*, 457, 1015
 Laor A., Draine B. T., 1993, *ApJ*, 402, 441
 Mackey J., Gvaramadze V. V., Mohamed S., Langer N., 2015, *A&A*, 573, A10
 Marston A. P., 1997, *ApJ*, 475, 188
 Meyer D. M.-A., Gvaramadze V. V., Langer N., Mackey J., Boumis P., Mohamed S., 2014, *MNRAS*, 439, L41
 Meyer D. M.-A., Mackey J., Langer N., Gvaramadze V. V., Mignone A., Izzard R. G., Kaper L., 2014, *MNRAS*, 444, 2754
 Meyer D. M. A., Mignone A., Kuiper R., Raga A. C., Kley W., 2017, *MNRAS*, 464, 3229
 Meyer D. M. A., Petrov M., Pohl M., 2020, *MNRAS*, 493, 3548
 Meyer D. M.-A., van Marle A.-J., Kuiper R., Kley W., 2016, *MNRAS*, 459, 1146
 Mignone A., Zanni C., Tzeferacos P., van Straalen B., Colella P., Bodo G., 2012, *ApJS*, 198, 7
 Miller G. J., Chu Y.-H., 1993, *ApJS*, 85, 137
 Moffat A. F. J., Marchenko S. V., Seggewiss W., van der Hucht et al. K. A. e. a., 1998, *A&A*, 331, 949
 Moffat A. F. J., Seggewiss W., 1979, *A&A*, 77, 128
 Munoz M., Moffat A. F. J., Hill G. M., Shenar T., Richardson N. D., Pablo H., St-Louis N., Ramiamanantsoa T., 2017, *MNRAS*, 467, 3105
 Prajapati P., Tej A., del Palacio S., Benaglia P., CH I.-C., Vig S., Mand al S., Kanti Ghosh S., 2019, *ApJ*, 884, L49
 Rate G., Crowther P. A., 2020, *MNRAS*, 493, 1512
 Renzo M., Zapartas E., de Mink S. E., Götzberg Y., Justham S., Farmer R. J., Izzard R. G., Toonen S., Sana H., 2019, *A&A*, 624, A66
 Sander A., Hamann W. R., Todt H., 2012, *A&A*, 540, A144
 Stock D. J., Barlow M. J., 2010, *MNRAS*, 409, 1429
 Toalá J. A., Guerrero M. A., 2013, *A&A*, 559, A52
 Toalá J. A., Guerrero M. A., Ramos-Larios G., Guzmán V., 2015, *A&A*, 578, A66
 Toalá J. A., Oskinova L. M., Hamann W. R., Ignace R. e. a., 2018, *ApJ*, 869, L11
 van der Sluis M. V., Lamers H. J. G. L. M., 2003, *A&A*, 398, 181
 van Marle A. J., Decin L., Meliani Z., 2014, *A&A*, 561, A152
 van Marle A. J., Langer N., García-Segura G., 2005, *A&A*, 444, 837
 Weaver R., McCray R., Castor J., Shapiro P., Moore R., 1977, *ApJ*, 218, 377
 Wilkin F. P., 1996, *ApJ*, 459, L31